Title

Magnetization Reversal of Three-Dimensional Nickel Anti-Sphere Arrays

Authors

Yu, Le

Yan, Zhongying

Yang, Han-Chang

et al.

Publication Date

2017

DOI

10.1109/lmag.2016.2616325

Peer reviewed

Nanomagnetics

Magnetization Reversal of Three-Dimensional Nickel Anti-sphere Arrays

L. Yu[1,4], Z. Y. Yan[1], H. C. Yang[1], X. Z. Chai[1,8], B. Q. Li[1], S. Moeendarbari[2], Y. W. Hao[2], D. Zhang[3], G. Feng[3], P. Han[4], D. A. Gilbert[5,6], Kai Liu[5,*], K. S. Buchanan[7], X. M. Cheng[1]

[1]*Department of Physics, Bryn Mawr College, Bryn Mawr, PA 19010, USA*
[2]*Department of Materials Science and Engineering, University of Texas at Arlington, Arlington, TX 76010, USA*
[3]*Department of Mechanical Engineering, Villanova University, Villanova, PA 19085, USA*
[4]*School of Electronic Science and Engineering, Nanjing University, Nanjing 210093, China*
[5]*Physics Department, University of California, Davis, CA 95616, USA*
[6]*National Institute of Standards and Technology, Gaithersburg, MD 20899, USA*
[7]*Department of Physics, Colorado State University, Fort Collins, CO 80523, USA*
[8]*School of Electric and Information Engineer, Zhongyuan University of Technology, Zhengzhou 450007, China*
**Fellow, IEEE*

Abstract—Three-dimensional anti-sphere arrays (3DAAs) of Ni have been fabricated using electrochemical deposition into self-assembled polystyrene sphere templates, which offers the advantage of straightforward scalability. Using the first-order reversal curve (FORC) method the magnetic reversal mechanism is identified from the characteristic features in the FORC distribution. A left-bending boomerang-like feature is observed in the thinnest sample and transforms to a ridge oriented along the local coercivity H_c axis with increasing sample thickness. This transformation identifies a change in the reversal processes from an exchange dominated domain-growth reversal to a localized weakly-interacting particle-like reversal. Micromagnetic simulations confirm the decrease in domain growth and increase of pinning behaviors as the thickness of the Ni 3DAAs structure increases, providing strong support to the FORC analysis and interpretation.

Index Terms—Nanomagnetics, three-dimensional anti-sphere arrays, first-order reversal curve, micromagnetic simulation

I. INTRODUCTION

Nanoscale magnetic materials, such as nanodots, nanowires, nanopillars, and nanostripes, have attracted considerable attention due to interest in both the fundamental properties and the potential applications. Three-dimensional anti-sphere arrays (3DAAs) have similarly been the focus of intensive research effort due to their use in photonic materials, and applications to sensors and high-capacity electrode materials. While the 2D antidot arrays are often fabricated by photolithography or template-based processes, efficient and low-cost fabrication of 3D anti-sphere array structures has been made possible by technical advances in electrochemical deposition using self-assembled colloidal polystyrene templates [Bartlett 2003]. The so-fabricated anti-sphere array materials with periodic structure and high surface-to-volume ratio provide an ideal system for studying the effect of dimensionality and morphology on magnetic properties [Zhukov 2006].

Probing the micromagnetic characteristics in a realistic 3D nanostructure system with interactions has been a long-standing challenge. Extensive work has been done on 2D magnetic antidot arrays [Zhukov 2006, Michea 2014], however, research to date on their 3D counterparts (i.e. multilayered anti-sphere arrays) has been limited to conventional magnetometry [Bartlett 2003, Zhukov 2006]. In this work we employ the first-order reversal curve (FORC) method [Mayergoyz 1986] to acquire detailed information about magnetization reversal behavior, especially irreversible switching. The FORC distribution is shown to transform from a left-bending boomerang-like feature to a ridge, oriented parallel to the local coercivity H_c axis, as the thickness of 3DAAs samples increases. This transformation signals a change in the reversal from a domain nucleation and growth reversal mechanism to a localized, weakly-interacting reversal. Micromagnetic simulations reveal the thickness dependent domain propagation behaviors and confirm our interpretation of the FORC features.

Corresponding author: X. M. Cheng (xcheng@brynmawr.edu).

II. MATERIALS AND METHODS

Ordered Ni 3D anti-sphere arrays (3DAAs) were fabricated by electrochemical deposition into colloidal crystal templates of self-assembled polystyrene spheres (PS) on Au-coated silicon wafers and the subsequent removal of the PS by dissolution in toluene [Eagleton 2004], as shown in Fig. 1 (a). The pore size is controlled by polystyrene sphere size. The top-view scanning electron microscopy (SEM) images [Fig. 1 (b)] show that the fabricated 3DAAs exhibit well-ordered hexagonal anti-sphere arrays with a pore size of 200 nm. Each anti-sphere formed has three regular dark regions that correspondto the contact with the three anti-spheres in the layer below. When viewed from the side (Fig. 1c), the anti-sphere arrays show symmetry that, along with the hexagonal arrangement of the top surface, is consistent with a face cubic center (FCC) arrangement, which agrees well with previous studies that have

reported the FCC arrangement as the main stack sequence in the 3DAA structure fabricated using self-assembled PS template [Bartlett 2003]. The cross-sectional SEM images [Fig. 1 (c)] show 3DAAs with pore size of 200 nm and layer numbers (defined as the thickness-to-pore-diameter ratio) of 0.5, 3 and 7.5, which were obtained by controlling the amounts of reduced nickel ion charges during the deposition step to be -0.5 C, -1.5 C and -5 C, respectively. 3DAAs samples with pore size of approximately 500 nm and layer numbers 0.5, 1.5, and 3.5 were also fabricated.

FIG. 1 HERE

The magnetization reversal process of the anti-sphere arrays was investigated using the FORC method, which is a powerful method to analyze the reversal behavior, especially the irreversible switching. It has been used previously to obtain information on reversal processes in a variety of structures, including nanowire arrays, thin films [Davies 2005], antidot arrays [Rahman 2009, Michea 2014], and magnetic skyrmions [Gilbert 2015]. To generate a FORC, the sample is first saturated in a positive field, and then the field is lowered to a reversal field H_r. Next the magnetization $M(H, H_r)$ is recorded while the applied field H is increased back to the saturation field in small steps. A series of such curves are recorded for progressively smaller H_r [See Fig. 2 (b) inset]. Together these curves probe the details of the reversal process; sweeping H_r probes the down-switching events and sweeping H probes the up-switching events.

The raw FORCs can be used to construct a FORC distribution to highlight the magnetic switching information contained in the raw data. The FORC distribution $\rho(H, H_R)$ [Fig. 2], which measures the dependence of the slope of the raw FORCs on the reversal field, is obtained from the second-order derivative of $M(H, H_r)$:

$$\rho = -\frac{1}{2}\frac{\partial^2 M\left(H, H_r\right)}{\partial H_r \partial H} \quad (1)$$

The FORC distribution can be transformed into a new coordinate system, where $H_c \equiv (H-H_r)/2$ is the local coercivity and $H_b \equiv (H+H_r)/2$ is the bias/interaction field. The new (H_c, H_b) coordinates represent a scaling and 45° rotation relative to the (H, H_r) coordinates. The purpose of this transformation is to identify a coordinate system reflective of the symmetries of the FORC feature. In this work we use the FORC technique, as a tool to identify specific reversal mechanisms within this complex, interconnected system.

FIG. 2 HERE

Magnetic measurements were performed at room temperature, in the in-plane geometry, using a vibrating sample magnetometer (VSM). FORCs were measured with a saturation field of 270 mT, in steps of ≈1 mT. The two dimensional FORC distributions [Fig. 2] were calculated using the FORCinel software suite [Harrison 2008].

To support our interpretations of the FORC distribution and help visualize the underlying magnetization reversal behaviors, micromagnetic simulations using OOMMF (Object Oriented Micromagnetic Framework) program [Donahue 1999] are performed using a 7 nm cubic mesh and bulk properties for polycrystalline Ni. The designed anti-spheres have a radius of 252 nm, and stack in an FCC sequence, with the (111) face parallel to the substrate and center-to-center spacing of 504 nm. The total area of the simulations is 2016 nm × 2016 nm, with a thickness of 252 nm, 819 nm and 1498 nm to simulate the 0.5 layer, 1.5 layer, and 3.5 layer samples, respectively. The simulated hysteresis loop spans a range of ±200 mT.

III. Results and discussion

A left-bending "boomerang"-like feature, identified by a horizontal arm with a narrow H_r distribution and an orthogonal arm with narrow H distribution, is observed in the FORC distribution for Ni 3DAAs with pore size of 200 nm and layer number of 3, as shown in Fig. 2 (b). Such a boomerang feature is typical of reversal by a domain nucleation and growth process [Gilbert 2016]. The horizontal FORC feature along H identifies domain growth under increasing applied field, after initial nucleation from positive saturation, highlighted by the red dashed box and oval in Fig. 2 (b) inset, respectively. The vertical FORC feature along H_r corresponds to domain re-nucleation after achieving (partial) negative saturation, highlighted by the blue dashed box and oval in Fig. 2 (b) inset, respectively [Davies 2004]. The fact that domain growth (horizontal feature) occurs at more negative values of the H (-10 mT < $\mu_0 H$ < +15 mT for example in panel (b)) than the domain nucleation (vertical feature, $\mu_0 H$ = +15 mT) identifies a strong tendency towards positive saturation, which suggests that a dominant exchange interaction is present within the system [Gilbert 2016].

FORC distributions of the 3DAAs with different layer numbers and pore sizes are shown in Fig. 2. With increasing sample thickness the FORC feature changes from the left-bending boomerang [Fig. 2 (a), (b), (d) and (e)] to a ridge oriented along the H_c axis. For the latter, horizontal and vertical ridges are still present but they meet at an angle that is much greater than 90° [Fig. 2 (c) and (f)]. The ridge parallel to H_c axis resembles that in a "particle" system with a distribution of intrinsic coercivities [Dumas 2007]. Interactions within these systems are manifested as distortions to the ridge features along the H_b axis in non-trivial ways [Gilbert 2014a, Béron 2011]. Therefore, the change in FORC distribution feature indicates that the dominant reversal mechanism changes from an exchange dominated domain nucleation-and-growth reversal to a localized weakly-interacting reversal as the thickness of the 3DAAs increases.

Micromagnetic simulations were conducted for Ni 3DAAs with the pore size of 500 nm in order to gain insight into the reversal behaviors in the 3DAAs structures, and to further explore the thickness dependent transition from domain-growth reversal to a localized, weakly-interacting reversal. The simulated region is considerably smaller than the extended antidot lattice films used in the experiment, but they can be used as a qualitative guide to the reversal process. Fig. 3 shows representative magnetic domain configurations during the reversal process as a function of decreasing applied field H. The reversal behavior observed in the bottom layer of each structure [Fig. 3 (a)] proceeds in a similar manner for all of the thicknesses. In all cases small regions reverse and then the reversal proceeds via domain expansion. The reversal generally appears to begin in the thinner regions near the voids, but once formed, the domains can propagate without much impedance in

this layer. Fig. 3 (a) also shows the domain configuration of representative upper layers in the structures that intersect two layers of voids and are hence much lower in density. For the sample with 1.5 layers, this layer still reverses via a domain expansion process, however, as shown in the spin distributions for both the 1.5 layers and 3.5 layer samples, small regions of perpendicular magnetization form in the most constricted regions due to the local out-of-plane shape anisotropy. As a result of the decreased density and presence of these out-of-plane regions, the reversal process proceeds in a more disconnected fashion in the upper regions of the sample. In the thickest sample (3.5 layers), more pinning sites (light and dark regions, which represent regions of perpendicular magnetization) are observed and the in-plane domains (blue and green regions) in the upper layers of the 3.5 layers are effectively disconnected from other in-plane domains. The stronger pinning in the upper layers of 3.5-layer sample can be observed more clearly in the cross-sectional domain configurations [Fig. 3 (b)]. Similar effects are observed in the 1.5-layer thick sample, however, the effect is less pronounced.

FIG. 3 HERE

The simulations suggest a general picture of the evolution of the reversal mechanism of the 3DAAs with sample thickness. In the thinnest sample and the bottom layer of the other models, reversal occurs by domain growth, and would be expected to form a boomerang FORC feature. In the thinnest samples, this is the dominant reversal mechanism. By comparison, the thickest sample possess a larger fraction of lower-density interconnected networks defined by the inter-spherical voids. These void spaces are only weakly connected at narrow vertex points, which provide pinning sites for domain walls. As a result, the reversal mechanism in the void-filled layers is a largely disconnected process that is entirely different from the manner in which the bottom layer and thinnest sample reverse. Since the samples were measured by VSM, the apparent reversal mechanism is a superposition of the two features, weighted by their magnetic fraction.

To further support this argument, the weight of the reversible and irreversible features can be compared. Specifically, for a thin 3DAAs, such as the 0.5 layer one, the sample can be considered as a film with divots and pyramids in/on it. On reducing the field from positive saturation it is expected that the film should remain largely saturated and reverse by domain propagation, as shown in the simulations and fingerprinted with FORC. By comparison, samples comprised predominantly of the spherical voids will experience significant reversible relaxation of the moments on the surface of the voids due to shape anisotropy. Thus the contribution from the reversible phase should increase with sample thickness - or conversely the irreversible fraction should decrease. The weight of the irreversible switching in the total switching behaviors, M_{irrev}/M_s, can be approximately obtained from the integrated weight of the FORC distribution and the saturation magnetization [Davies 2005, Gilbert 2014b]:

$$M_{irrev} / M_s \approx \frac{1}{M_s} \sum \rho(H_c, H_b) \Delta H_c \Delta H_b \qquad (2)$$

This formula gives an irreversible weight of 0.40, 0.32 and 0.35 for the 200 nm pore size Ni 3DAAs with the layer number of 0.5, 3, and 7.5, respectively, confirming the thinnest sample possesses the largest irreversible fraction.

IV. CONCLUSION

In conclusion, we have investigated the magnetic reversal process in the Ni 3DAAs samples using the FORC method and micromagnetic simulations. The transformation of the FORC feature from a left-bending boomerang (0.5 layer, 3 layers with 200 nm pore size and 0.5 layer, 1.5 layers with 500 nm pore size) to a ridge parallel to the H_c axis (7.5 layers with 200 n pore size and 3.5 layers with 500 nm pore size) reveals a transition from an exchange dominated domain growth reversal process to a localized, weakly-interacting reversal process as thickness increases. Micromagnetic simulations show that domain propagation dominates in the lowest quasi-continuous layer, whereas the reversal process becomes more localized in the void-heavy upper layers, which result in the change in the reversal mechanism with thickness that is consistent with the FORC results.

ACKNOWLEDGMENT

Work at Bryn Mawr College is supported by the National Science Foundation (NSF) under Grant No. 1207085. Work at UC Davis is supported by the NSF (DMR-1008791 and DMR-1543582). Work at UT Arlington is supported by the NSF Grant No. 1207377. Work at CSU was supported by DOE-BES ER46854. Le Yu is supported by the China Scholarship Council fellowship.

REFERENCES

Bartlett P N, Ghanem M A, El Hallag I S, de Groot P, Zhukov A A (2003), "Electrochemical deposition of macroporous magnetic networks using colloidal templates," *J Mater. Chem.*, vol. 13, pp. 2596-2602, doi: 10.1039/b304496c.

Béron F, Pirota K R, Vega V, Prida V M, Fernandez A, Hernando B, Knobel M (2011), "An effective method to probbe local magnetostatic properties in a nanometric FePd antidot array," *New J. Phys.* vol. 13, 013035 doi:10.1088/1367-2630/13/1/013035.

Davies J E, Wu J, Leighton C, Liu K (2005), "Magnetization reversal and nanoscopic magnetic-phase separation in $La_{1-x}Sr_xCoO_3$," *Phys. Rev. B*, vol. 72, 134419, doi: 10.1103/PhysRevB.72.134419.

Davies J E, Hellwig, O, Fullerton, E E, Denbeaux, G, Kortright J B, Liu, K (2004) "Magnetization reversal of Co/Pt multilayers: Microscopic origin of high-field magnetic irreversibility," *Phys. Rev. B*, vol. 70, 224434, doi: 10.1103/PhysRevB.70.224434.

Donahue M J, Porter D G, OOMMF User's Guide, Version 1.2a6, NIST, Gaithersburg, MD. In this work, following material parameters are used in the simulations: exchange coefficient $A=9\times10^{-12}$ J/m; saturation magnetization $M_s=4.9\times10^5$ A/m; cubic anisotropy constant $K_1=-5.7\times10^3$ J/m^3 with easy axis in <111> directions and hard axis in <100> directions.

Dumas R K, Li, C-P, Roshchin I V, Schuller I K, Liu K (2007), "Magnetic fingerprints of sub-100 nm Fe nanodots", *Phys. Rev. B*, vol. 75, 134405, doi: 10.1103/PhysRevB.75.134405.

Eagleton T S, Searson P C (2004), "Electrochemical synthesis of 3D ordered ferromagnetic nickel replicas using self-assembled colloidal crystal templates," *Chem. Mater.*, vol. 16, no. 24, pp. 5027-5032, doi: 10.1021/cm0491781.

Gilbert D A, Zimanyi G T, Dumas R K, Winklhofer M, Gomez A, Eibagi N, Vicent J L, Liu K (2014a), "Quantitative decoding of interactions in tunable manomagnet arrays using first order reversal curves," *Sci. Rep.*, vol. 4, 4204, doi: 10.1038/srep04204.

Gilbert D A, Liao J-W, Wang L-W, Lau J W, Klemmer T J, Thiele J-U, Lai C-H, Liu K (2014b) "Probing the A1 to L10 transformation in FeCuPt using the first order reversal curve method," *APL Mater.*, vol. 2, 086106, doi:10.1063/1.4894197.

Gilbert D A, Maranville B B, Balk A L, Kirby B J, Fischer P, Pierce D T, Unguris J, Borchers J A, Liu K (2015) "Realization of Ground State Artificial Skyrmion

Lattices at Room Temperature", *Nat. Commun.*, vol 6, 8462, doi: 10.1038/ncomms9462.

Gilbert D A, Liao J W, Kirby B J, Winklhofer M, Lai C H, Liu K (2016), "Magnetic Yoking and Tunable Interactions in FePt-Based Hard/Soft Bilayers", *Sci. Rep.*, vol. 6, 32842, doi:10.1038/srep32842.

Harrison R J, Feinberg J M (2008), "FORCinel: An improved algorithm for calculating first-order reversal curve distributions using locally weighted regression smoothing," *Geochem. Geophy. Geosy.*, vol. 9, no. 5, Q05016, doi:10.1029/2008GC001987.

Mayergoyz I D (1986), "Mathematical models of hysteresis," *IEEE Trans. Magn.*, vol. 22, no. 5, pp. 603-608, doi: 10.1021/ic049522w.

Michea S, Palma J L, Lavín R, Briones J, Escrig J, Denardin J C, Rodríguez-Suárez R L (2014), "Tailoring the magnetic properties of cobalt antidot arrays by varying the pore size and degree of disorder," *J. Phys. D: Appl. Phys.*, vol. 47, no. 33, 335001, doi:10.1088/0022-3727/47/33/335001.

Rahman M T, Dumas R K, Eibagi N, Shams N N, Wu Y C, Liu K, Lai C H (2009), "Controlling magnetization reversal in Co/Pt nanostructures with perpendicular anisotropy," *Appl. Phys. Lett.*, vol. 94, 042507, doi: 10.1063/1.3075061 .

Zhukov A A, Goncharov A V, de Groot P A J, Ghanem M A, Bartlett P N, Boardman R, Fangohr H, Novosad V, Karapetrov G (2006), "Oscillatory thickness dependence of the coercive field in magnetic three-dimensional antidot arrays," *Appl. Phys. Lett.*, vol. 88, no. 6, 062511, doi: 10.1063/1.2171792.

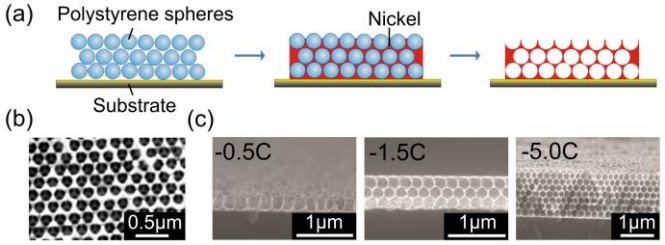

Fig. 1. (a) Schematic illustrations showing the fabrication process of Ni 3DAAs by electrodepositing into a self-assembled template of polystyrene spheres (PS). (b) Top-view SEM images of Ni 3DAAs with a pore size of 200 nm and the reduced Ni ion charge of -5.0 C, where the light and dark areas are Ni and voids, respectively. (c) Cross-sectional SEM images of Ni 3DAAs with the same pore size as (b). The reduced Ni ion charge used during the deposition, ranging from -0.5 C to -5.0 C, results in increasing sample thickness.

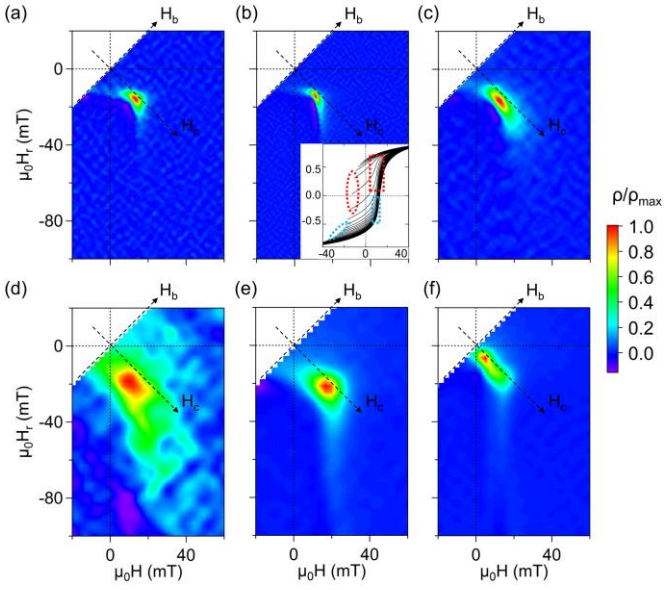

Fig. 2. FORC distributions of Ni 3DAAs with different layer numbers and pore sizes: (a) 0.5 layer, (b) 3 layers and (c) 7.5 layers with pore sizes of approximately 200 nm; and (d) 0.5 layer, (e) 1.5 layers and (f) 3.5 layers with pore sizes of approximately 500 nm. For Ni 3DAAs with both pore sizes, the FORC feature changes from a left-bending "boomerang" to a ridge parallel to the H_c axis as thickness increases. The significantly increased width of the distribution in (d) is due to the sample inhomogenieties. The inset in (b) shows a selected family of normalized FORC's for this sample within -40 mT < $\mu_0 H$ < 40 mT. Red (blue) dashed circle and rectangle mark the regions that correspond to the H_r and H of the horizontal (vertical) branch of the FORC distribution.

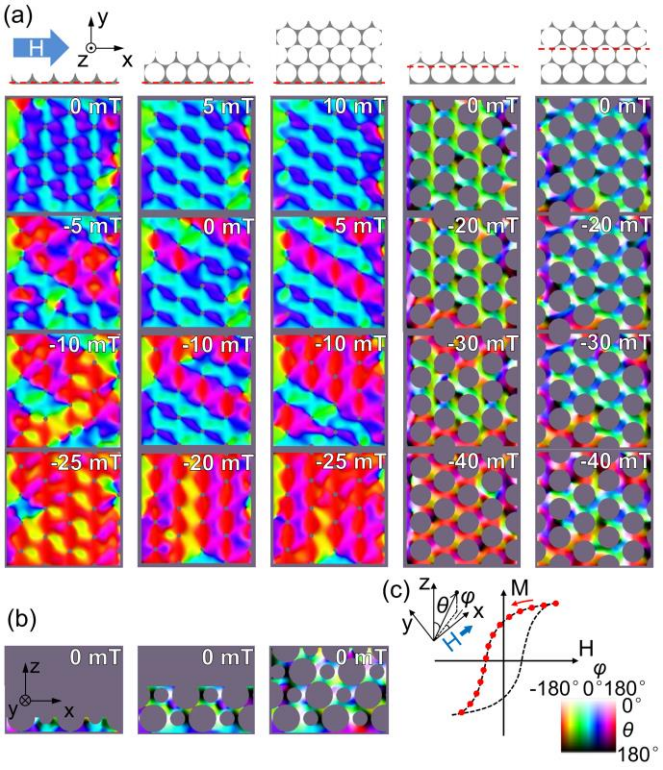

Fig. 3. Magnetic domain configurations obtained from micromagnetic simulations. (a) Top-view images of the spin distributions in the bottom, quasi-continuous layers are shown for samples that involve 0.5, 1.5, and 3.5 layers of spheres with a pore size of 500nm. The distributions are also shown for selected higher-up, lower-density layers. The slice positions are marked by red dashed line in the side-view cartoon above each column. The domain configurations exhibit rapid domain propagation in the bottom layers and the spins are mainly in-plane, whereas the slices taken near the void exhibit heavier pinning in areas that are thicker and regions with a significant out-of-plane tilt are observed. (b) Cross-sectional images of the remanent state show regions with perpendicular magnetization (light and dark regions) in the thicker samples that impede lateral domain propagation, especially for the thickest samples (3.5 layers). The spin distributions shown represent the progression of the magnetization under a decreasing magnetic field H, as illustrated in (c), where H is applied at an angle of $\theta = 90^o$ (in-plane) and $\varphi = 0^o$. The color represents the in-plane φ angle and the shading reflects the out-of-plane angle θ as shown in the insets of (c).